Anal. Bioanal. Electrochem., Vol. 15, No. 7, 2023, 568-586
https://www.doi.org/10.22034/abec.2023.706510

Analytical & Bioanalytical Electrochemistry

Full Paper

Performance of Thiosemicarbazone to Protect Copper Against Corrosion in A 3% NaCl Solution, Experimental and Theoretical Studies

Biari Aomar,[1,*] Dermaj Ahmed,[1] Mostafa Doubi,[1] Erramli Hamid,[1] Driss Chebabe,[2] Hajjaji Najat,[1] and Bakkali Said[3]

[1]*Laboratory of Organic Chemistry, Catalysis and Environment, Faculty of Sciences, Ibn Tofail University, BP 133, 14000, Kenitra, Morocco*
[2]*Laboratory of Materials Engineering for the Environment and Natural Resources, Faculty of Sciences and Techniques, Moulay Ismail University of Meknes, B.P 509, Boutalamine, 52000, Errachidia, Morocco*
[3]*Departement of Chemistry, Faculty of Sciences of El Jadida, Chouaib Doukkali University, PO. BOX: 20, El Jadida, Morocco*

*Corresponding Author, Tel.: 212661534679
E-Mail: ammarbiari67@gmail.com

Received: 4 April 2023 / Received in revised form: 4 July 2023 / Accepted: 20 July 2023 / Published online: 31 July 2023

Abstract- In recent years, the use of inhibitors remains the most adopted method for the protection of metals and alloys against aggressive media. The objective of this work is to test the inhibiting effect of thiosemicarbazone noted TSC vis-à-vis the corrosion of copper in a 3% NaCl solution. In this study, we used stationary (potentiodynamic measurements), and transient (impedance diagrams) methods in the absence and presence of different concentrations of inhibitors. Polarization curves showed that thiosemicarbazone acts as a mixed inhibitor. Its effect results in a potential shift towards the anodic direction and a significant decrease in current density. Electrochemical impedance diagrams show the capacitive behavior of copper in a 3% NaCl solution. The addition of the inhibitor at different concentrations leads to a change in the corrosion mechanism with an increase in the polarization resistance, consequently, the inhibitory efficiency increases and reaches 95% for a concentration of 10^{-3} M. This testifies to the significant protective effect of thiosemicarbazone against copper corrosion in 3% NaCl.

Keywords- Copper; Corrosion; Inhibition; Thiosemicarbazone; Inhibitor TSC

1. INTRODUCTION

The semicarbazones and thiosemicarbazones are organic products that have excellent coordination and complexing ability with transition elements. They can be used in chemistry as organic inhibitors [1,2]. These products, which can be synthesized by several different methods, have the following general formula.

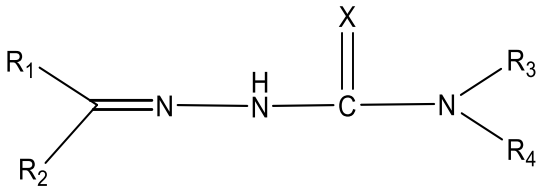

Scheme 1. The general formula of TSC

R_1, R_2, R_3, and R_4 are alkyl or aryl groups, (X=O) for semicarbazones and (X=S) for thiosemicarbazones [3-7].

These compounds have a wide application in pharmacology, biology, chemistry [8-11], and corrosion inhibitors of carbon steel [12-14]. The efficiency of these compounds shows their ability to form complexes with various transition metals. The presence of heteroatoms such as sulfur, nitrogen, and oxygen in their structures is an important factor for their better activity against corrosion [15].

Thanks to its mechanical properties, thermal and electrical conductivity as well as its good solderability and corrosion resistance, copper is widely used in many industrial units, particularly in heat exchangers, electrical appliances, and cooling systems.

The good corrosion resistance of copper can be explained in two ways: in an acid environment, copper is more resistant because the standard potential of Cu/Cu(I) is more positive than the potential for hydrogen release; whereas in a neutral environment, an adherent film is formed on the surface of the metal by the corrosion products and acts as a barrier against the corrosive environment [16].

In the presence of certain ions such as Cl^-, copper becomes very sensitive to corrosion. So, it is essential to protect it. Among the methods of protection of metals against corrosion, organic inhibitors are widely used, and it is within this framework that the objective of our study falls.

In our work, we aimed to synthesize, and identify the product thiosemicarbazone, denoted TSC, and make its application as a copper corrosion inhibitor in NaCl 3%. The study of its inhibiting power against the corrosion of copper in a solution of NaCl 3% was carried out using stationary techniques, namely polarization curves and transient techniques, in particular electrochemical impedance spectroscopy.

2. EXPERIMENTAL CONDITIONS

2.1. Material and medium:

In our study, copper of purity 99.999% (Goodfellow). The material used in this. The corrosive medium chosen is a solution of NaCl 3% prepared from pure solid NaCl and distilled water. This choice is justified by the fact that the situation is under the influence of an aggressive marine environment.

2.2. Electrochemical instrumentation:

The intensity-potential curves are drawn using a potentiostat (Biologic SP200) with a three-electrode electrochemical cell: The reference electrode is a saturated calomel type; the auxiliary is a platinum electrode while the working electrode is a pure copper sample, cut in the form of a cylinder insulated laterally by an epoxy resin, leaving a surface of $1cm^2$. Before each experiment, the surface of the sample is polished with 600, 1200 and 2400 grit abrasive paper, then degreased and dried.

The polarization measurements anodic and cathodic were plots separately starting from the corrosion potential towards respectively more cathodic and more anodic potentials with a scanning speed of 5 mv s^{-1}.

The inhibition efficiency (Ei) was calculated according to the following equation:

$$Ei = \frac{(Icorr - Icorr(inh))}{Icorr} x\ 100 \qquad \text{(Eq. 1)}$$

The electrochemical impedance measurements are performed in a Faraday cage with a potentiostat adapted to the measurement of low currents and high impedance (Biologic SP200). The excitation signal has an amplitude of 5mV with a frequency sweep from 100KHz to 10mHz at a rate of 10 points per decade.

2.3. Inhibitor

The product chosen as inhibitor is thiosemicarbazone (TSC), synthesized from benzaldehyde and thiosemicarbazide in the presence of ethanol by the following chemical reaction:

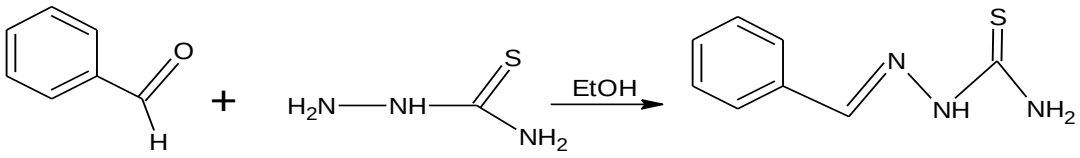

Scheme 2. Synthesized of TSC

This product, obtained with a good yield is characterized and identified based on proton NMR and 13 carbon NMR.

Spectral characteristics:

- ^{1}H NMR (500 MHz, DMSO-D_6): (NH) s, 2.456 ppm; (phényl) m, 7,356-8 ppm; (H iminiqie) s, 8.157 ppm.
- ^{13}C NMR (125 MHz, DMSO-D_6): (C phényl) 127.817-134,661 ppm; (Carbone iminique) 142.820 ppm; (carbone thioamidique) 178.460 ppm.

3. RESULTS AND DISCUSSION

3.1. Stationary measurements

The cathodic and anodic polarization measurements were obtained after one hour of immersion at corrosion potential in a 3% NaCl solution with a stirring speed of 600 rpm at different concentrations of thiosemicarbazone; they are shown in Figure 1.

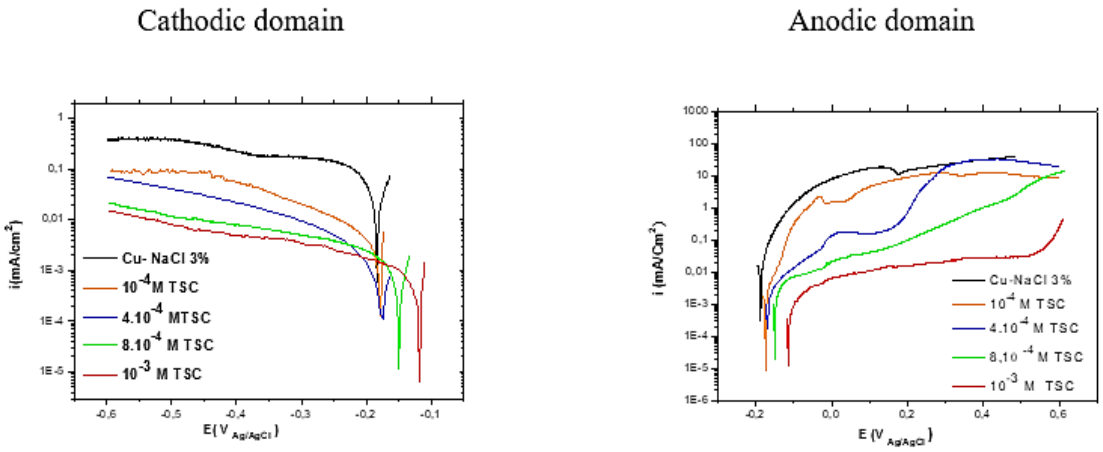

Figure 1. Cathodic and anodic current-voltage curves of copper in NaCl 3% in the presence of different concentrations of TSC

The examination of the cathodic domain shows that:

In the blank test, the current density increases near the corrosion potential and tends to stabilize by forming a plateau due to the diffusion of dissolved oxygen according to the following reaction:

$$O_2 + 2\,H_2O + 4e^- \leftrightarrows 4HO^- \qquad \text{(Eq. 2)}$$

Then the kinetics of the corrosion is controlled by the diffusion resulting from the reduction of oxygen which plays a primordial role in the mechanism of the corrosion. This cathodic reaction is considered as the driving force of corrosion [17-19].

The addition of TSC is accompanied by a displacement of the corrosion potential towards the positive direction and a significant decrease in the current density with the increase in its concentration. This decrease appears in the whole cathodic domain. In the vicinity of E_{corr} , the current density goes from 22,03 µA.cm^{-2} in the absence of an inhibitor to 1,02 µA.cm^{-2} in the presence of 10^{-3} M TSC. This explains the protective effect of this product in this area.

For all the concentrations of TSC, the variation of the current density on a semi-logarithmic scale presents a linearity that follows Tafel's law, which allows the calculation of current densities by extrapolation of Tafel's lines [20-22].

Without an inhibitor, the anodic curves show a rapid increase in current density near the corrosion potential indicating the selective dissolution of copper in this medium according to the following reaction:

$$Cu \leftrightarrows Cu^{2+} + 2e^- \quad \text{(Eq. 3)}$$

The mechanism of anodic dissolution in the presence of chlorides is well-known and characterized by the following two reactions [23-25]:

$$Cu + Cl^- \leftrightarrows CuCl_{ads} + e^- \quad \text{(Eq. 4)}$$

$$CuCl_{ads} + Cl^- \leftrightarrows CuCl^{-2} \quad \text{(Eq. 5)}$$

At the highest anodic overvoltages, the current density tends to stabilize, forming a current plateau of about 10 mA/cm^2. This value is very high to signify the passivation of the metal, so it is attributed to corrosion products. The addition of the TSC inhibitor at different concentrations shows a very significant change in the polarization curves, as well as the anodic reaction rate. Indeed, the addition of TSC leads to a shift of corrosion potential toward positive values and a strong decrease in the anodic current density. This decrease is more marked when the TSC concentration increases. For 10^{-3}M concentration, a current plateau is observed with a value of about 2µA/cm^2, which corresponds to the formation of an inhibiting film on the metal surface with a protective character [26]. For more anodic potentials, the polarization curves join the curve of the blank test, which means the deterioration of the film formed by the desorption of inhibitor from the metal surface [27-29]. The anodic polarization curves in the presence of different concentrations of TSC confirm the enhancement of the passive state of the metal by completely changing the dissolution reaction of copper in the solution of NaCl 3%. The kinetic parameters of the cathodic and anodic curves are shown in Table 1.

The analysis of this table shows a shift of the corrosion potential toward the anodic direction and a significant decrease in the corrosion current density with the inhibitor concentration. This decrease can be explained by the formation of an inhibiting film on the metal surface. The inhibitory efficiency of TSC calculated by the relation (Eq. 1) is about 95%, testifying this effect. The obtained results showed the TSC act as a good inhibitor of copper in a solution of NaCl 3% by preventing its dissolution in the corrosive medium.

Table 1. Electrochemical parameters issued from polarization measurements

[TSC](M)	Cathodic domain			Anodic domain			E (%)
	E_{corr} (V_{Ecs})	I_{corr} (μAcm^{-2})	Bc (mv^{-1})	E_{corr} (V_{Esc})	I_{corr} (μAcm^{-2})	Ba (mv^{-1})	
0	-0.288	22.03	-175.23	-0,285	22.53	275.36	-
10^{-4}	-0.195	4,98	-149,89	-0,184	5,02	195,55	77,39
4.10^{-4}	-0.180	3.72	-148.67	-0.176	3.77	191.07	83,11
$8.\ 10^{-4}$	-0.149	1.91	-138.84	-0.152	1.96	153.75	91,33
10^{-3}	-0.128	1.02	-140.47	-0.124	1.04	147.14	95,36

3.2. Adsorption isotherm

The study of the adsorption isotherm is useful to understand the nature of the inhibitor-metal interaction and the kinetics of adsorption.

To know the adsorption mode of the TSC on the metal surface of copper in 3% NaCl, we traced the variation of the concentration as a function of the recovery rate. The results obtained are illustrated in Figure 2.

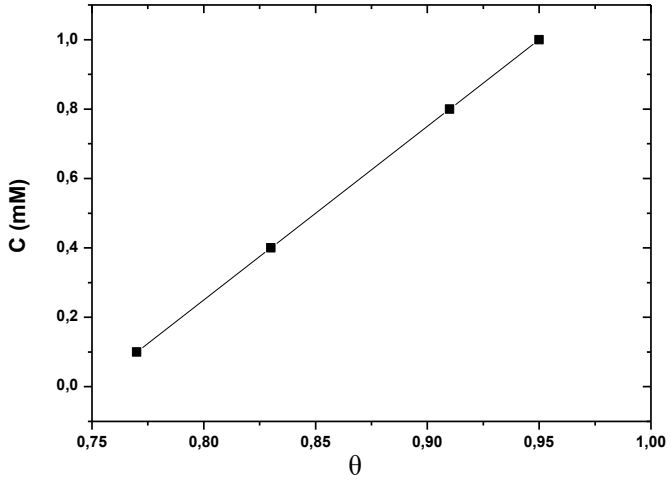

Figure 2. Langmuir adsorption isotherm of TSC in 3% NaCl at 298K

From this figure, it can be seen that the variation of the concentration as a function of the recovery rate obeys the Langmuir isotherm. The thermodynamic parameters were calculated from the following equations [30-33]:

$$\frac{C\text{inh}}{\theta} = C\text{inh} + \frac{1}{K} \qquad K_{ads} = 1/55{,}5 \exp(-\Delta G°_{ads}/RT) \qquad \text{(Eq. 6,7)}$$

The value of ΔG°ads explains the nature of the adsorption: if $\Delta G°_{ads}$ is less than -40 kJ/mol, the inhibitor adsorbed on the surface of the metal undergoes chemical adsorption; When the value of $\Delta G°_{ads}$ is between -40 and -20 kJ/mol, the inhibitor is adsorbed in a mixed manner. Finally, if $\Delta G°_{ads}$ exceeds -20 kJ/mol, the inhibitor is adsorbed by physisorption [34-36]. The value of $\Delta G°_{ads}$ of TSC which is -34.47 kJ/mol, shows that our inhibitor is adsorbed on the copper surface according to the mixed adsorption.

3.3. Electrochemical impedance measurements

3.3.1. Concentrations effect

To better understand the phenomenon that governs the interface copper/solution of NaCl 3% we have used transient measurements namely the electrochemical impedance diagrams. The results obtained are illustrated in Figure 3.

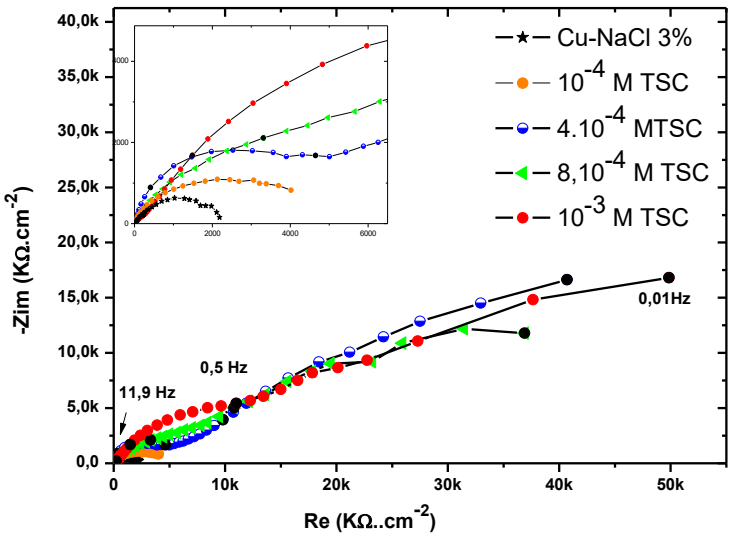

Figure 3. Electrochemical impedance diagrams of copper in a solution of 3% NaCl in the presence of different concentrations of TSC

After one hour of immersion at the corrosion potential, the electrochemical impedance diagrams recorded in a frequency range from 100 KHz to 10 mHz show that:

In the absence of a TSC inhibitor, the shape of the electrochemical impedance diagram shows the appearance of two capacitive loops which are difficult to discern. In agreement with other authors [37, 38] the loop at high frequencies is attributed to the phenomenon of charge transfer (R_t-C_d), and the loop at low frequencies is attributed to the diffusion phenomenon (R_d-T_d). The modeling of this diagram by the Ec-Lab software (Biologic instrument) confirmed the presence of these two loops (Table 2). The intersection of the Nyquist diagram with the real

axis obtained by extrapolation at zero frequency gives a value of the polarization resistance Rp of the order of 2167.80 Ωcm^2.

The equivalent electrical circuit corresponding to the electrochemical impedance diagram of copper in a 3% NaCl solution is shown in Figure 4.

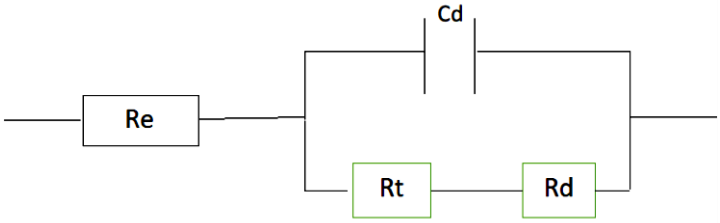

Figure 4. The equivalent electrical circuit of impedance diagram of copper in a 3% NaCl solution

The addition of TSC at different concentrations in the corrosive medium reveals a capacitive behavior with a different diagram shape than in the case of copper alone. This can be explained by a change in the mechanism of the interfacial corrosion process. The electrochemical impedance diagrams show a significant increase in polarization resistance in the presence of the inhibitor. They reveal the presence of at least two different contributions.

The modeling of these diagrams by the Ec-Lab program does not correspond to two R-C circuits; so, the addition of a third constant was necessary to model these diagrams. Thus, as a result of the application of E_c-Lab, we have:

A contribution at high frequencies (R_f - C_f) associated with the dielectric character of the film formed by the corrosion products reinforced by the presence of inhibitor and ionic conduction through the film pores.

A contribution (R_t-C_d) attributed to the capacitance of the double layer at the electrolyte/copper interface at the bottom of the pores, coupled with the charge transfer resistance.

A contribution (R_d) corresponds to the diffusion phenomenon [39].

The parameter fitting results for the (R_f-C_f) and (R_t-C_d) pairs derived from the plots in Figure 3 are shown in Table 2.

Analysis of Table 2 shows that at very high frequencies, the diameter of the capacitive loop is of the order of 1120, 1481, 1650, and 2491 Ωcm^2 for TSC concentrations of 10^{-4}; 4×10^{-4}; 8×10^{-4} and 10^{-3} M respectively. The associated capacities (2.23; 1.91; 1.7 and 0.83 µF.cm^{-2}) are low compared to that usually attributed to the double layer (50 µF.cm^{-2}). This is in agreement with the hypothesis of the formation of a thick film due to the presence of the TSC inhibitor. The protective effect increases with increasing inhibitor concentration.

At medium frequencies, the obtained loop was attributed to charge transfer. There is a significant increase in the associated resistance, its value is of the order of several kΩcm^2 (from 9 to 20 kΩcm^2). The value of the charge transfer resistance increases by a factor of 14 in the

presence of 10^{-3} M in TSC, compared to the control. This shows that TSC has a significant effect on decreasing the corrosion rate of copper in NaCl 3%.

Table 2. Fitting parameters for the two parallel R-C circuits in Figure 3

[TSC] (M)	R_0 ($\Omega.cm^2$)	C_f ($\mu F.cm^2$)	R_f ($\Omega.cm^2$)	C_d ($\mu F.cm^{-2}$)	R_t ($k\Omega.cm^2$)	IE %
0	12,84	-----	-----	152	1,21	----
10-4	12,06	2,23	1120	45,64	5,67	78,65
4.10^{-4}	11,54	1,91	1481	42,48	8,15	85,15
8.10^{-4}	13,72	1,73	1650	41,01	16,93	92,85
10^{-3}	15,02	0,83	2492	37,08	19,98	93,94

The Morse of the third capacitive loop is consistent with impedance linearity observed at very low frequency. This may indicate the existence of a third-time constant that can be attributed to the diffusion phenomenon [40].

The equivalent electrical circuit corresponding to the electrochemical impedance diagram of copper in a 3% NaCl solution in the presence of the TSC inhibitor is shown in Figure 5.

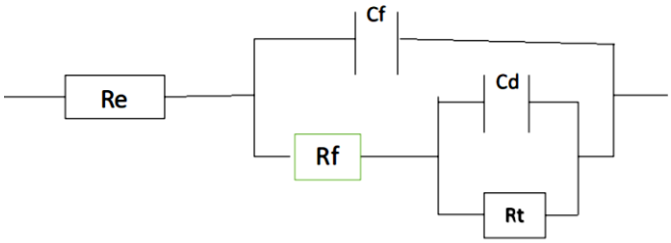

Figure 5. The equivalent electrical circuit of electrochemical impedance diagram of copper in a 3% NaCl solution in the presence of the TSC inhibitor

The inhibitory efficiency calculated by the relation (6):

$$E_i = \frac{Rt(inh) - Rt(0)}{Rt(inh)} \times 100 \qquad (Eq.\ 8)$$

where:

- Rt (inh) is the charge transfer resistance in the presence of the inhibitor.
- Rt (0) is the charge transfer resistance in the absence of the inhibitor.

The efficiency increases with the inhibitor concentration, reaching 94% (Table 3) for the concentration of 10^{-3} M, confirming the protective character of TSC.

Table 3. TSC quantum chemical descriptors at 6-311+G(D,P) level.

E_{HOMO}(eV)	E_{LUMO}(eV)	ΔE (eV)	μ(Debey)	Δ*N*
-0,230	-0,074	0,157	2,449	27,645

This result shows that TSC has a protective effect on copper in a solution of NaCl 3%. Its effect is reflected in the formation of a relatively thick and compact inhibitor film on the copper surface. This film acts as a barrier against aggressive ions. Its protective power is of the order of 94% for the concentration of 10^{-3}M chosen as the best concentration for the following tests. This efficiency value agrees with the one obtained from stationary measurements.

3.3.2. Immersion time effect

The examination of the effect of immersion time on the inhibition efficiency of TSC at 10^{-3} M, by electrochemical impedance measurement, is illustrated by Figures 6 and 7.

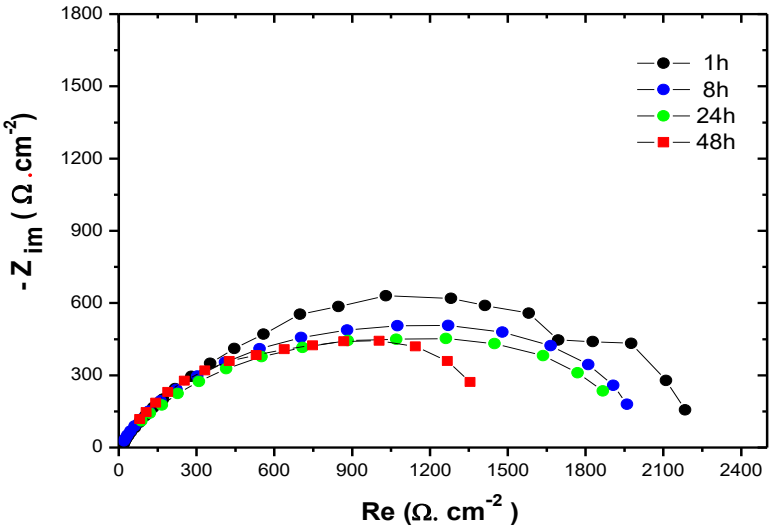

Figure 6. Electrochemical impedance diagrams of copper in a solution of NaCl 3% at different immersion times

The electrochemical impedance diagrams at different immersion times show the same shape, which shows that the corrosion mechanism does not change. These diagrams highlight a capacitive behavior of copper in a solution of NaCl 3% with a decrease in polarization resistance as a function of immersion time. It goes from 2179 Ω.cm^2 after 1h to 1500 Ω.cm^2 after 48h of immersion. This decrease is explained by the attack of copper in the aggressive medium especially by chlorides. This reflects an increase in the corrosion rate of copper.

In the presence of 10^{-3}M TSC, the electrochemical impedance diagrams have the same appearance with a significant increase in polarization resistance. It increases from 19 KΩ.cm^2 to 50 KΩ.cm^2. This increase can be explained by the formation of a thick and compact inhibitor film and is reinforced by the increase in the immersion time. The low-frequency loop shows a linear part that can be attributed to diffusion through a solid barrier represented by the inhibitor film formed with a thick and compact character.

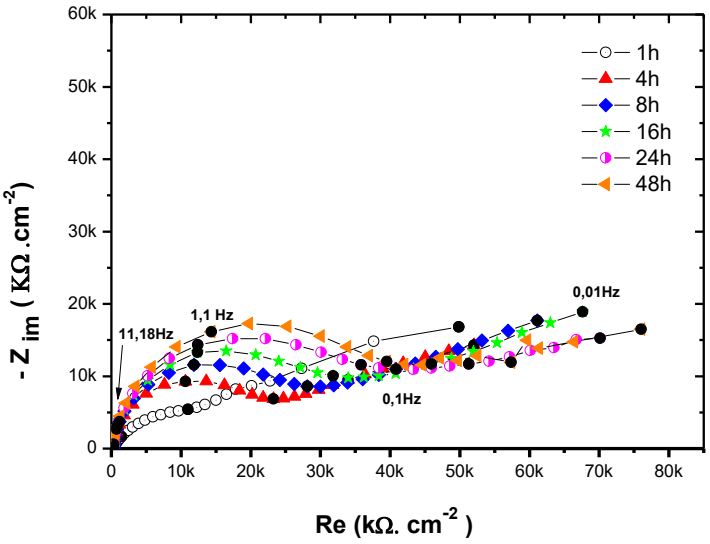

Figure 7. Effect of immersion time on the electrochemical impedance diagrams of the copper/NaCl 3% interface in the presence of 10^{-3} M TSC

3.4. Theoretical study

3.4.1. Quantum chemical calculations

All DFT calculations were performed using B3LYP method and the 6–311G+ basis set in the presence of water as solvent using Gaussian 09 Revision D-0.

The reactivity of the TSC was investigated by the evaluation of the HOMO, LUMO and band gap ΔEg energies, the dipole moment (μ), and the electron transfer parameters (ΔN) based on Eqs:

$$\Delta E_g = E_{LUMO} - E_{HOMO} \quad \text{(Eq. 9)}$$

$$\Delta N = \frac{\chi_{Cu} - \chi_{TSC}}{2(\eta_{Cu} - \eta_{TSC})} \quad \text{(Eq.10)}$$

Where χC u = 4.48 eV/mol and ηCu= 0 eV/mol.

$$\chi_{TSC} = -\frac{E_{HOMO} + E_{LUMO}}{2} \quad \text{(Eq. 11)}$$

$$\eta_{TSC} = \frac{E_{LUMO} - E_{HOMO}}{2} \quad \text{(Eq. 12)}$$

The local reactivity of the TSC molecule was analyzed by calculating Fukui indices from the values of the natural population analysis using the following formulas [41]:

$$f^{-} = q_K(N) - q_K(N-1) \quad \text{(Eq. 13)}$$

For an electrophilic attack,

$$f^{+} = q_K(N+1) - q_K(N) \quad \text{(Eq. 14)}$$

For a nucleophilic attack.

Where $q_K(N-1)$, $q_K(N)$ and $q_K(N+1)$ are the populations of the atom k, in the cationic, neutral and anionic species respectively.

The adsorption behavior of TSC on the copper electrode was elucidated by the dynamic molecular simulations using the Forcite module implemented in the Materials Studio package. The interaction between the TSC and the studied surface in the NaCl environment was simulated in a box (30,7× 30,7× 39.1 $Å^3$) containing a six-layer Cu (111) surface, a single TSC molecule, $10Na^+$, $10Cl^-$ and 500 H_2O molecules.

The simulation was performed at 298 K under periodic boundary conditions with the canonical ensemble (NVT) and using the COMPASS II force-field. The time step and the simulation time were 1.0 fs and 200 ps respectively.

The adsorption energy E_{ad} and binding energy E_{bd} are calculated according to:

$$E_{ad} = E_T - (E_{TSC} + E_{Su/so}) \quad \text{(Eq. 15)}$$

$$E_{bd} = -E_{ad} \quad \text{(Eq. 16)}$$

where E_T presents the total energy; E_{TSC} is the total energy of the TSC molecule and $E_{Su/so}$ indicates the total energy of the metal surface and the solution without the TSC molecule.

3.4.2. Theoretical considerations

Quantum chemistry and molecular dynamics simulation studies were undertaken to link the experimental results with the TSC conceptual parameters. Figure 8 describes the optimized geometric structure and the distribution of the HOMO and LUMO orbitals of the studied molecule. As can be seen, the molecule has a flat geometry (Figure 8a). Such a configuration increases the TSC interaction with the metal if this molecule stands parallel to the metallic surface. The HOMO and LUMO electron clouds are known to provide information about a molecule's electron-donating and electron-acquiring abilities [38]. In our findings, the HOMO orbital is located on the linear part of the TSC (Figure 8b). Whereas the LUMO orbital is spread over the whole skeleton of the studied molecule (Figure 8c).

The energy gap (ΔE_g) is a key parameter that informs on the capacity of a molecule to adsorb on the metal surface. In fact, molecules with low ΔE_g are easily adsorbed on the metallic surface and thus show high anti-corrosion performance.

The investigated molecule can strongly adsorb the metal surface and consequently ensure effective corrosion protection of Cu since the ΔEg value of TSC is very low compared, in similar conditions, to other potential copper corrosion inhibitors [42-44].

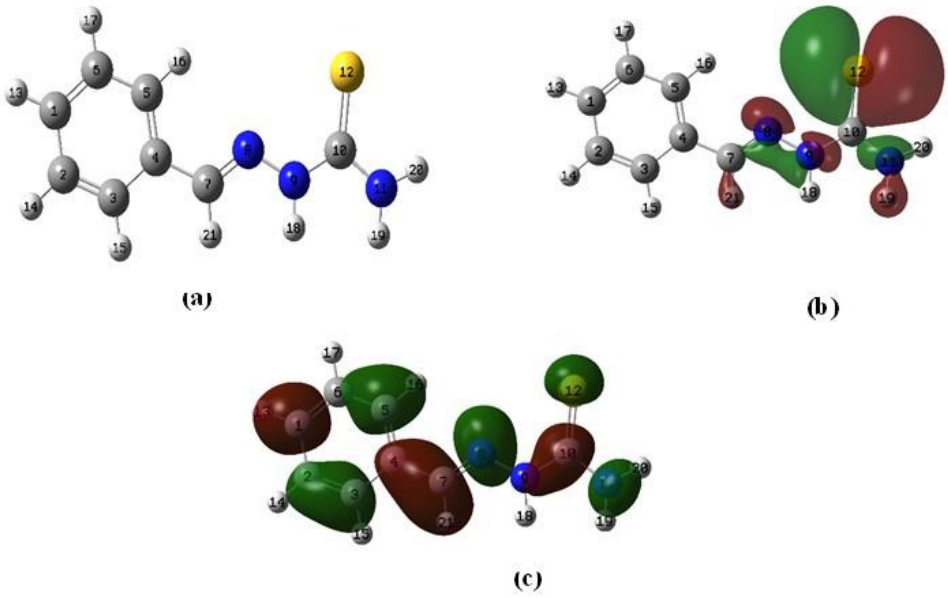

Figure 8. (a) Optimized structure of TSC. Frontier molecular orbitals (b) HOMO, (c) LUMO

The cause-and-effect relationship between the dipole moment (μ) and inhibitive performance is not well established. Indeed, some researchers reported that molecules with low dipole moments are effective inhibitors [45], whereas others suggested that inhibitor efficacity increases with increasing μ [46]. The positive sign of the electron transfer parameter (ΔN) suggests that the TSC molecule provides electrons to the unoccupied sites of the Cu surface. This reinforces the adsorption of TSC on the study surface.

The electrostatic potential map (MEP) highlights the areas in a molecule of negative (red), positive (bleu) and zero MEP (green).

The theoretical MEP in Figure 9 shows that the region with high electron density (red area) is around the sulfur atom.

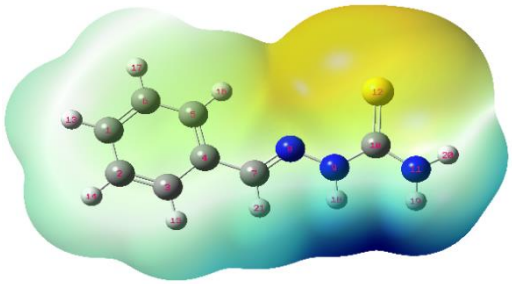

Figure 9. Electrostatic potential map of TSC

Table 4. Fukui indices for TSC calculated at 6-311+G (D, P) level

Atom		f(-)	f(+)
1	C	-0,0174	0,1226
2	C	0,0001	0,0322
3	C	0,0152	0,0488
4	C	-0,0114	0,0271
5	C	0,0112	0,1026
6	C	0,0014	0,0055
7	C	0,0427	0,1554
8	N	-0,0178	0,1465
9	N	0,0443	-0,0105
10	C	-0,0129	0,0196
11	N	0,0536	0,0347
12	S	**0,7522**	0,1677

Further information on the local activity of the TSC is provided by Fukui functions (Table 4). The atom with a high f(-) value shows a nucleophilic character, whereas this one with a high f(+) value has an electrophilic character.

As shown in Table 4, S12 is the preferable site for an electrophile attack. The nucleophilic attack can occur preferentially at S12, C7, N8, C1 and C5 atoms. Note that S12 could play a vital role in the adsorption of the TSC molecule on the metal surface since it has both donating and accepting abilities.

3.4.3. Molecular dynamic (MD) simulation

Figure 10 shows the low-energy adsorption configuration of the TSC molecule on the Cu (111) surface. As can be seen, the molecule is flatly adsorbed on the metallic surface. Such a configuration provides maximum surface coverage and ensures good corrosion protection. Moreover, the highly negative value of the adsorption energy highlights the strong and spontaneous adsorption of the TSC on the copper surface.

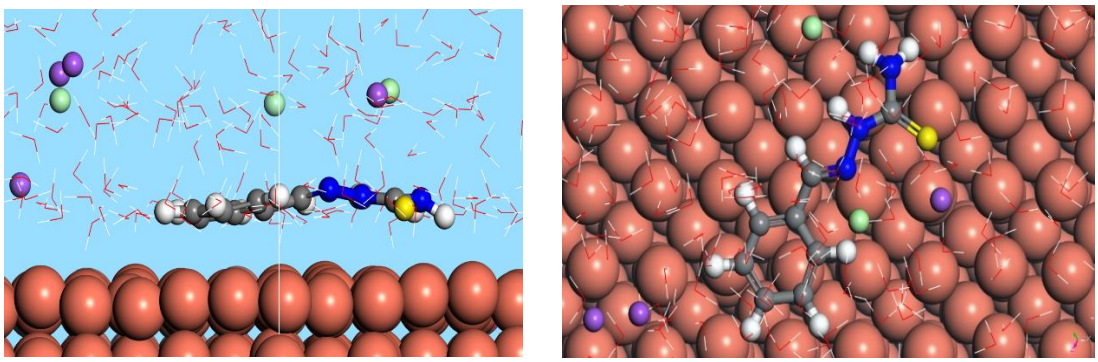

Figure 10. The most suitable configurations of adsorption TSC on Cu (111) surface in the aqueous phase at 298K. a) Side view. b) Top view

The radial distribution function (RDF) is used to depict the nature of the TSC adsorption on the copper. Indeed, the literature reports that the chemisorption mechanism is more likely when the densest peak is between 1 and 3.5 Å. Conversely, if this peak appears at a distance greater than 3.5 Å, physisorption is more favourable. As can be seen, the position of the first peak in Figure 11 suggests probable chemical adsorption occurring within the studied system between TSC and Cu.

Table 5. Adsorption and binding Energies of TSC on Cu surface

	E_{ad}(kJ/mol)	E_{bd}(kJ/mol)
TSC	-390,79	390,79

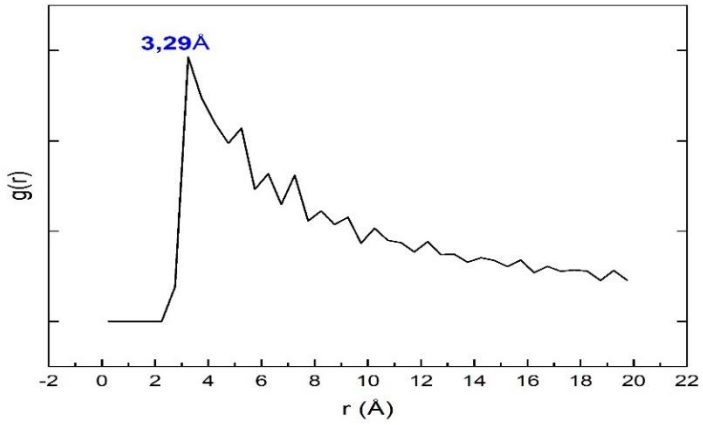

Figure 11. RDF curve for the TSC molecule on Cu surface

The non-covalent interactions (NCI) analysis allows mapping the weak interactions in 2D and 3D representations using the electron density (ρ) and the reduced density gradient (RDG) expressed as follows:

$$RDG = \frac{1}{2(3\pi^2)^{1/3}} \frac{|\nabla\rho|}{(\rho)^{4/3}} \quad \text{(Eq. 17)}$$

The NCI plots are colour-coded blue-green-red to represent strong attractive and van der Waals interactions, as well as steric repulsion.

The equilibrium state obtained from the previous molecular dynamic simulation was examined with non-covalent interactions (NCI) analysis (Figure 12) to get more information on the interaction between TSC and Cu surface.

The green colour in Figure 12 reveals the existence of the Van der Waals interactions between all the TSC atoms and the copper surface. So, the inhibitory performance of TSC can also be related to the non-covalent interactions involved in the studied system. This finding supports the parallel arrangement of the TSC on the Cu surface. Indeed, it was stated that the

horizontal disposition of the inhibitor on the metal surface gives rise to the physisorption or mixed chemisorption and physisorption [47,48].

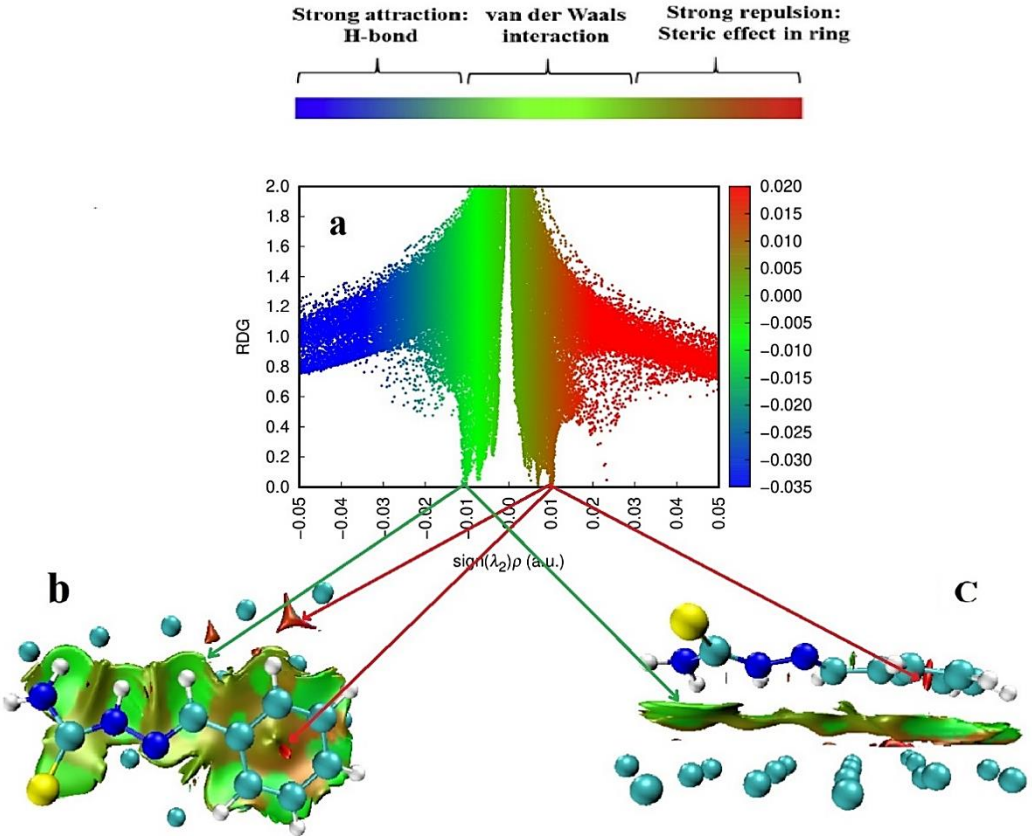

Figure 12. The 2D and 3D RDG plots of TSC/ C (1 1 1) system. a) 3D b) 2D side view, c) 2D top view

4. CONCLUSION

The studied thiosemicarbazone has electron donating atoms. Sulfur is among these atoms which have a major importance in the metal-ligand bonding. The polarization results obtained revealed that the TSC compound behaved as a mixed type of corrosion inhibitor. Its inhibitory effect against copper corrosion in NaCl 3% showed that it inhibits both anodic and cathodic reactions. This effect results in a decrease of the current density and a shift of the corrosion potential towards more noble values.

In the anodic domain, the action of TSC is manifested by the appearance of a current plateau (passivity current is clearly apparent) at high inhibitor concentrations. Compared to the control, in the same potential domain (passivation domain) where the anodic current density value is about 10 mA/cm2. Thus, the inhibitor protects the copper satisfactorily in a neutral chloride and aerated environment even under anodic polarization. This protection is maintained for immersion times up to 48 hours. An inhibitory efficiency of 94% is achieved at a concentration of 10^{-3} M.

The electrochemical impedance spectra obtained at the corrosion potential also revealed a capacitive behavior of copper due to the inhibitory effect of TSC. Its effect results in an increase of polarization resistance and in the formation of a relatively compact and thick film, which is probably favored by the corrosion products. It appears from the computational approaches that: The TSC has multiple active sites. Chemisorption and physisorption could occur between the TSC and the Cu (111) surface, according to the RDF and NCI analyses.

Between the TSC molecule and the Cu (111) surface, spontaneous adsorption occurs in which the studied molecule remains parallel to the copper surface. So, theoretical findings corroborate the experimental results.

Declarations of interest

The authors declare no conflict of interest in this reported work.

REFERENCES

[1] T.S. Lobana, R.B. Sharma, G. Awa, and S. Khanna, Coordination Chem. Rev. 253 (2009) 977.
[2] I. Lukovits, A. Shaban, and E. Kálmán, Electrochim. Acta 50 (2005) 4128.
[3] D.X. West, A. Liberta, S.B. Padhye, R.C. Chikate, P.B. Sonawane, A.S. Kumbhar, and R.G. Yerande, Coord. Chem. Rev. 123 (1993).
[4] N.A. Mangalam, and M.R.P. Kurup, Spectrochim. Acta 71 (2009) 2040.
[5] E. Rodríguez-Argüelles, C. López-Silva, J. Sanmartín, P. Pelagatti, and F. Zani, J. Inorg. Biochem. 99 (2005) 2231.
[6] T.S. Lobana, R. Sharma, G. Bawa, and S. Khanna, Polyhedron 91 (2015) 89.
[7] G.K. Kumar, G.E. Chavarria, A.K. Charlton-Sevcik, W.M. Arispe, M.T. MacDonough, T.E. Strecker, S.E. Chen, B.G. Siim, D.J. Chaplin, and M.L. Trawick, Bioorg. Med. Chem. Lett. 20 (2010) 1415.
[8] M.S. Almutairi, A.S. Zakaria, P.P. Ignasius, R.I. Al-Wabl, and I.H. Joe, J. Mol. Struct. 1153 (2018) 333.
[9] W.X. Hu, W. Zhou, C.N. Xia, and X. Wen, Bioorg. Med. Chem. Lett. 16 (2006) 2213.
[10] K.S. Jacob, and G. Parameswaran, Corros. Sci. 52 (2010) 224.
[11] K.F. Khaled, Electrochim. Acta 55 (2010) 5375.
[12] J.S. Casas, M.S. García-Tasende, J. Sordo, Coord. Chem. Rev. 209 (2000) 197.
[13] H. Beraldo, Quim. Nova 27 (2004) 461.
[14] X. Li, S. Deng, and H. Fu, Corros. Sci. 53 (2011) 302.
[15] H. Belagra, Study and characterization of the protection of copper and copper-zinc alloy by self-assembled thin layers of alkane thiols. Effect of sulphide species. Thesis from University of Mohamed Boudiaf, Algeria (2013).

[16] N. Perez: Electrochemistry and Corrosion Science, Kluwer Academic Publishers, Boston. (2004) http://ebooks.kluweronline.com.
[17] E. Poorqasemi, O. Abootalebi, M. Peikari, and F. Haqdar, Corros. Sci. 51 (2009) 1043.
[18] Y. Qiang, S. Zhang, L. Guo, X. Zheng, B. Xiang, and S. Chen, J. Corr. Sci. 119 (2017) 68.
[19] B. Trachli, M. Keddama, H. Takenouti, and A. Srhiri, J. Progress in Organic Coatings 44 (2002) 997.
[20] A. Dermaj, N. Hajjaji, S. Joiret, K. Rahmouni, A. Srhiri, H. Takenouti, and V. Vivier, Electrochim. Acta 52 (2007) 4654.
[21] A. Dermaj, D. Chebabe, N. Hajjaji, V. Vivier, and J. Rrec, Res. Rev. Electrochem. 4 (2013) 147.
[22] R.P. Ferreira, C.C.F. Nascimento, G.S. Reis, E.S. Silva, and S.F. Rodrigues, Mater. Sci. and Applications 11 (2020) doi: 10.4236/msa.2020.114015.
[23] D. Chebabe, A. Dermaj, H. Erramli, and N. Hajjaji, J. Anti-Corrosion Methods and Materials 61 (2014) 281.
[24] M. Damej, D. Chebabe, M. Benmessaoud, A. Dermaj, H. Erramli, N. Hajjaji, and A. Srhiri, J. Corrosion Eng. Sci. Technol. 50 (2015) 103.
[25] Y. Qiang, S. Zhang, L. Guo, X. Zheng, B. Xiang, and S. Chen, J. Corr. Sci. 119 (2017) 68.
[26] H. Benassaoui, A. Dermaj, D. Chebabe, H. Erramli, M. Damej, and N. Hajjaji, J. Organic Chem. 11-12 (2015) 433.
[27] D. Chebabe, M. Damej, A. Dermaj, A. Oubair, M. Benassaoui, H. Erramli , N. Hajjaji, and A. Sghiri Anal. Bioanal. Chem. Res. (2020) 389.
[28] B. Trachli, Thèse Doctoral, university pierre and marie curie, Paris, France (2001).
[29] C. Gabrielli, M. Keddam, N. Portail, P. Rousseau, H. Takenouti, and V. Vivier, J. Phys. Chem. B 110 (2006) 20478.
[30] J.B. Jorcin, H. Krawiec, N. Pébère, and V. Vignal, Electrochim. Acta 54 (2009) 5775.
[31] L.L. Liao, S. Mo, J.L. Lei, H.Q. Luo, and N.B. Li, J. Colloid Interf. Sci. 474 (2016) 68.
[32] Y. Wang, Y. Zuo, X. Zhao, and S. Zha, Appl. Surf. Sci. 379 (2016) 98.
[33] E. Alibakhshi, M. Ramezanzadeh, G. Bahlakeh, B. Ramezanzadeh, M. Mahdavian, and M. Motamedi, J. Mol. Liq. 255 (2018) 185.
[34] N. El Hamdani, R. Fdil, M. Tourabi, C. Jama, and F. Bentiss, Appl. Surf. Sci. 357 (2015) 1294.
[35] A.E.A.S. Fouda, S.E.D.H. Etaiw, M.M. El-bendary, and M.M. Maher, J. Mol. Liq. 213 (2016) 228.
[36] Sudheer, and M.A. Quraishi, Corros. Sci. 70 (2013) 161.
[37] M. Benmessaoud, K. Es-Salah, A. Kabouri, N. Hajjaji, H. Takenouti, and A. Srhiri, Mater. Sci. Applications 2 (2011) 276.

[38] Y. Shi, L. Chen, S. Hou, S. Zhang, X. Wang, P. Dong, F. Gao, and L. Hongru, Colloids and Surfaces A 656 (2022) 130501.
[39] D.Q. Huong, T. Duong, and P.C. Nam, ACS Omega 4 (2019) 14478.
[40] S. Ghufran, A.M.B. Jassim, S.N. Aiyah, H.S. Mohanad, M.K. Mustafa, A.A. Haider, M.R. Ahmed, and L. Peng, Inorganic Chem. Commun. 142 (2022) 109650.
[41] S. Bakkali, M. Cherkaoui, A. Boutouil, M.R. Laamari, M. Ebn Touhami, M. Belfakir, A. Zarrouk, Surfaces and Interfaces 19 (2020) 100480.
[42] V. Simona, B.G. Camelia, B. Roxana, L.C. Raluca, S. Zohreh, T. Milad, R. Keyvan, I. Javier, and M.S. Ricardo, Electrochim. Acta 398 (2021) 139282.
[43] S.C. Dheeraj, M.A. Quraishi, C. Carrière, A. Seyeux, B. Marcus, and A. Singh, J. Mol. Liq. 289 (2019) 111113.
[44] B. Benzidia, M. Barbouchi, R. Hsissou, M. Zouarhi, H. Erramli, and N. Hajjaji, Curr. Res. in Green and Sustainable Chem. 5 (2022) 100299.
[45] X. Cheng, T. Bochuan, Z. Shengtao, and L. Wenpo, J. Taiwan Institute of Chem. Eng. 139 (2022) 104532.
[46] Z. Wenjun, L. Wenpo, T. Bochuan, L. Jia, and C. Jida, J. Taiwan Institute of Chem. Eng. 128 (2021) 417.
[47] S.A. Ohoud, and W. Nuha, J. Saudi Chem. Soc. 26 (2022) 101566.
[48] K. Anton, K. Natasˇa, P. Sebastijan, F. Matjazˇ, L. Antonija, and M. Ingrid, Chem. PhysChem. 12 (2011) 3547.